Romano *et al. Soft Sci* 2024;4:31
DOI: 10.20517/ss.2024.24

Soft Science

Research Article

Open Access

Check for updates

Tunable soft pressure sensors based on magnetic coupling mediated by hyperelastic materials

Chiara Romano[1], Daniela Lo Presti[1,2], Sergio Silvestri[1], Emiliano Schena[1,2], Carlo Massaroni[1,2,*]

[1]Department of Engineering, Università Campus Bio-Medico di Roma, Rome 00128, Italy.
[2]Fondazione Policlinico Universitario Campus Bio-Medico, Rome 00128, Italy.

[*]**Correspondence to:** Dr. Carlo Massaroni, Department of Engineering, Università Campus Bio-Medico di Roma, Via Alvaro del Portillo, Rome 00128, Italy. E-mail: c.massaroni@unicampus.it

How to cite this article: Romano C, Presti DL, Silvestri S, Schena E, Massaroni C. Tunable soft pressure sensors based on magnetic coupling mediated by hyperelastic materials. *Soft Sci* 2024;4:31. https://dx.doi.org/10.20517/ss.2024.24

Received: 22 Jun 2024 **First Decision:** 23 Jul 2024 **Revised:** 13 Aug 2024 **Accepted:** 31 Aug 2024 **Published:** 9 Sep 2024

Academic Editor: YongAn Huang **Copy Editor:** Dong-Li Li **Production Editor:** Dong-Li Li

Abstract

Recent advances in pressure sensors have garnered significant interest due to their promising applications in healthcare, robotics and wearable technology. In these fields, there is an ever-increasing demand for soft sensors that can conform to complex surfaces, such as the human body. However, current sensors often face limitations in measurable pressure ranges and customization involves complex manufacturing processes. In this study, we introduce an innovative solution for producing soft pressure sensors with varying maximum detection pressures. By utilizing a magnetic transduction mechanism and different hyperelastic materials, we have developed sensors that can adapt to irregular surfaces. These sensors measure a wide range of pressures, from ultra-low to medium, and offer variable stiffness, sensitivity, and measurement ranges. The sensors we manufactured exhibit a detection range from 6.8 to 77.4 kPa, a sensitivity range between -5.1 × 10^{-2} and -0.4 × 10^{-2} kPa^{-1}, a short recovery time of 0.4 s, low hysteresis values during repeated loading/unloading cycles, and stable response over thousands of pressure cycle. Proof-of-concept experiments validated the sensors' suitability for breathing monitoring and finger tap detection, highlighting their potential in medical and robotic applications. The results demonstrate a robust strategy for controlling the performance of soft pressure sensors, positioning them as promising candidates for diverse pressure sensing applications.

Keywords: Soft sensors, pressure sensing, wearable sensors, breathing monitoring

INTRODUCTION

In recent years, pressure sensors have attracted considerable interest due to their potential in diverse applications, ranging from healthcare to robotics. The demand for sensitive pressure sensing media is increasing significantly[1-3]. Their versatility is a major reason for this interest; for instance, when embedded in wearable chest straps, pressure sensors can measure breathing activity[4,5], or heart rate by sensing the small displacements generated by cardiac mechanics on the chest surface[6]. Additionally, these sensors are utilized in robotics for tactile sensing[7] and human motion monitoring[8], and in clinical applications, such as in anesthesiology, to detect the epidural space using the loss of resistance method[9].

The main limitation of traditional pressure sensors is their lack of flexibility, which has encouraged the scientific community to further investigate this field[10-12]. Thus, there is a growing need for tunable and flexible solutions capable of addressing different types of stimuli and accurately detecting dynamic pressure across a wide range- from ultra-low (< 1 kPa), low (1-10 kPa), medium (10-100 kPa), to high (> 100 kPa) - without compromising sensitivity[13,14]. Recent advances have introduced several innovative sensing solutions, and the concept of soft sensors has emerged[15-17], especially in human-machine and wearable electronics[18,19]. Various sensing elements have been proposed, featuring different structures and transduction mechanisms, including capacitance[20-22], piezoresistivity[23-25], and piezoelectricity[10,26,27].

Among these, piezoresistive flexible pressure sensors have been widely studied due to their simple operating principle. However, they face limitations such as low sensitivity, nonlinearity, high hysteresis, poor stability, and unsuitability for low-pressure ranges[7,23,28]. Conversely, capacitive sensors have gained significant attention due to their advantageous characteristics[29,30], including low sensitivity to temperature and humidity, low power consumption, and highly repeatable response[31]. However, they are typically suitable for high-pressure range applications[32] and are limited by poor linearity, and susceptibility to parasitic capacitance[31].

In this context, the magnetic transduction mechanism offers several advantages, such as linearity, reduced hysteresis, high repeatability and ease of fabrication[7,28,33]. This last factor is particularly noteworthy, as it contrasts with the previously discussed transduction mechanisms that typically require complex and challenging manufacturing processes, thereby complicating any modifications to their measurement range[34,35]. In this context, integrating air chambers into the deformable elements of piezoresistive or capacitive pressure sensors has shown promising potential for adjusting their stiffness[22,36-38]. However, the impact of these factors, especially their shape, on soft magnetic sensors remains unexplored. Building on these insights, we developed pressure sensors consisting of a Hall sensor and a soft element embedding a magnet. Our study was designed to enhance the tunability of soft magnetic pressure sensors through variations in the shape and material of the soft element. This methodology aims to extend the maximum detectable pressure range of these sensors, thereby broadening their applicability without necessitating changes to the fundamental magnetic and electronic architecture. We produced and metrologically characterized cylindrical-shaped sensors, implementing a Finite Element Method (FEM) model. These sensors were realized using five materials with varying stiffnesses and three different shapes: a solid cylinder, a cylindrical air chamber, and a domed air chamber. Lastly, we demonstrated the applicability of the produced sensors across various fields, including healthcare and robotics. This was achieved by recording finger-induced pressures (contact, soft touch, pressing), finger tapping, and chest deformations for non-intrusive measurement of breathing at different respiratory frequencies.

EXPERIMENTAL

Design and fabrication

We designed magnetic soft pressure sensors [Figure 1A and in Supplementary Section 1]. Each sensor comprises the following components: (i) a Hall effect sensor; (ii) a magnet (NdFeB, N45) with axial magnetization (dimensions: 1 mm height, 1 mm diameter); and (iii) a soft polymeric medium. While the Hall sensor and magnet remained unchanged, the polymeric medium varied in shape and material to modulate the sensor's stiffness. Externally, the polymeric medium was cylindrical (height: 8 mm, diameter: 8 mm), with variations in the internal configuration: 1. lacking an inner air chamber (FULL shape); 2. featuring a domed inner air chamber (DOM shape); and 3. having a cylindrical inner air chamber (CIL shape). We employed Ecoflex 00-50 (Eco50) and Ecoflex 00-30 (Eco30), along with three custom materials. These custom materials were formulated by mixing Eco30 with Silicone Thinner at different concentration levels: 10% (Eco30t10), 20% (Eco30t20), and 25% (Eco30t25) of the total volume. Ecoflex™ rubbers, which are platinum-catalyzed silicones, consist of two components: Part A and Part B. To produce the soft sensors, these components were combined in a 1A:1B volumetric ratio, according to the manufacturer's guidelines. For Eco30t10, Eco30t20, and Eco30t25, 0.050, 0.100, and 0.125 g of Silicone Thinner, respectively, were added to decrease the sensors' stiffness. All materials were then degassed using a vacuum/pressure pump (model VCP 130, VWR International, LLC, PA, USA) for ten minutes to eliminate air bubbles. Next, negative molds were created using 3D-printed polylactic acid (PLA). The prepared materials were poured into the molds, and the magnet was embedded in the soft medium at 2 mm from the Hall sensor. The entire sensor production process is illustrated in Supplementary Figure 1. When a uniform force is applied to the upper surface of the soft medium, it deforms, reducing the gap between the magnet and the Hall sensor [Figure 1B]. This compression alters the magnetic field detected by the Hall sensor [Figure 1C]. The relationship between the magnetic field (B) in milliTesla (mT) and the sensor's output (V_{out}) is expressed by:

$$B = 20.47 \cdot \left(2 \cdot \frac{V_{out}}{V_{dd}} - 1\right) \quad (1)$$

where V_{dd} is the supply voltage and 20.47 mT represents the sensor's full scale.

Metrological characterization of soft pressure sensors

To metrologically characterize each soft sensor, we measured the sensor output using a data acquisition board (DAQ NI USB-6009, National Instruments) under both quasi-static loads and loading/unloading cycles generated by a tensile testing machine (Instron 3365). We set the compressive displacement of the moving plate to 3 mm (equivalent to 37.5% compressive strain), with a displacement rate of 2 mm/min. We conducted five tests and calculated the expanded uncertainty using a t-Student distribution with four degrees of freedom and a 95% confidence level. To assess the sensor's response to repeated compressive loading, we subjected it to ten loading and unloading cycles at four different moving plate displacement rates (0.1, 0.2, 0.8, and 1 Hz).

Materials characterization and finite element analysis of soft pressure sensors

To investigate the influence of sensor shape and materials on stiffness, we employed a FEM model. Each custom-made material underwent initial characterization under both tension and compression conditions to determine its characteristic coefficients. Compression and tensile tests were conducted following ISO 7743:2017 standards and ASTM D412:2006 guidelines. A comprehensive description of these procedures is available in Supplementary Section 2. Five specimens were fabricated according to ISO 7743:2017 and five according to ASTM D412:2006 for each material. Mechanical testing was performed using an Instron 3365 tensile testing machine, adhering to the respective standard guidelines. Stress and strain data were then

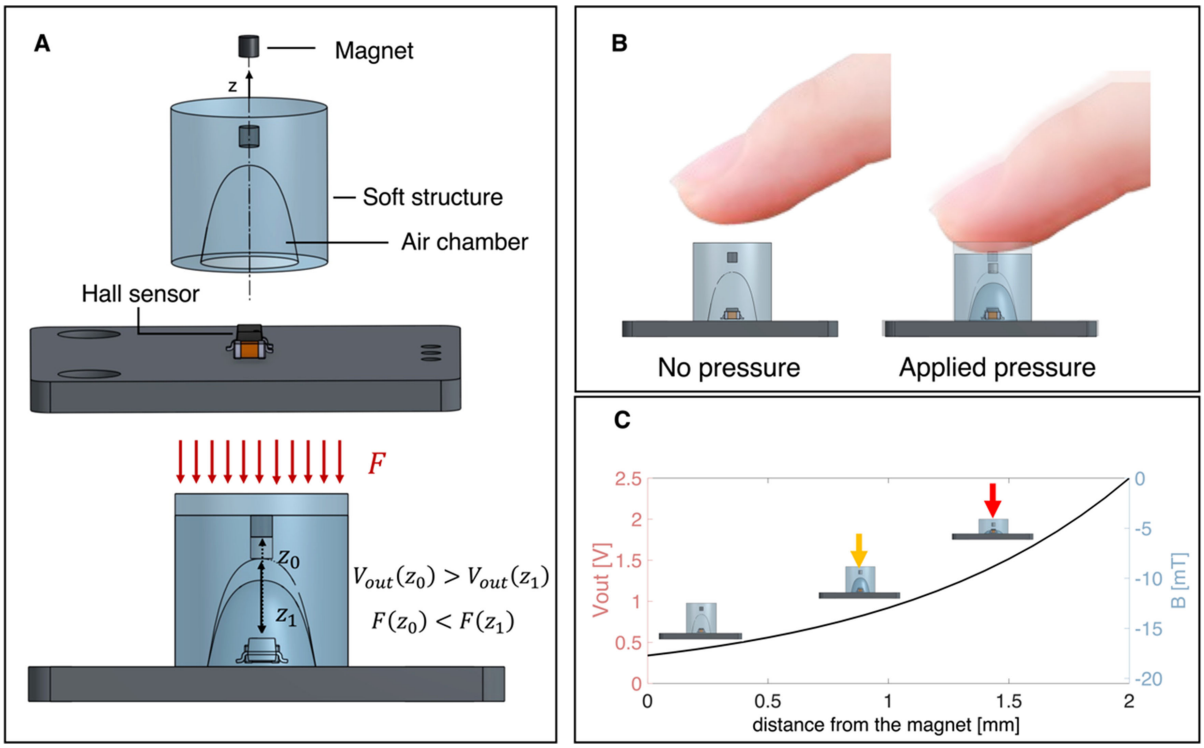

Figure 1. Soft magnetic pressure sensor. (A) Structure of the sensor and schematization of the operating principle; (B) Schematic representation of the mechanical behavior of the sensors under external pressures; (C) V_{out} and B at different distances between magnet and Hall sensor (according to Equation 1).

input into the simulation platform (COMSOL Multiphysics, USA), where the Yeoh model was employed to determine material coefficients that best fit the experimental data. Detailed coefficients for the five materials are provided in Supplementary Table 1 in Supplementary Section 3. After characterizing the five materials, finite element analysis was conducted using the Structural Mechanics and AC/DC modules within COMSOL Multiphysics. The geometries of each soft medium (FULL shape, DOM shape, and CIL shape) were initially created using CAD software (Onshape) and subsequently imported into COMSOL Multiphysics. The Yeoh third-order hyperelastic material model and its parameters (c1, c2, and c3) were utilized to simulate the hyperelastic behavior of the five materials described previously. A displacement of 1 mm (corresponding to 12.5% deformation) was imposed on the upper surface of the silicone structure, and the resulting pressure distribution was recorded.

Breathing and finger-tapping detection

To evaluate the effectiveness of the proposed sensor structure, two sensors with varying stiffness levels were tested in different application scenarios. The study was conducted on a 35-year-old male volunteer, in accordance with the guidelines of the Declaration of Helsinki. The study received approval from the Institutional Ethics Committee of Università Campus Bio-Medico di Roma (09/19 OSS ComEt UCBM). The participant provided written consent, including permission for photography and video recording during the testing sessions, as well as consent for using recorded data for publication purposes.

In the first proof-of-concept experiment, a pilot study was conducted with a volunteer to evaluate the sensors' capability in estimating breathing from chest wall movements. For this purpose, the sensor was integrated into a wearable band using double-sided Velcro and positioned inside the band so that the soft part of the sensor faced the subject's chest when worn. Before the experiment, the band was worn by the

volunteer with the sensor centered on the sternum at the height of the seventh rib. Subsequently, the volunteer was asked to follow the experimental protocol involving phases of uncontrolled breathing, apneas performed at the end of inhalation and exhalation, quiet breathing, and fast breathing. Each protocol phase aimed to assess the sensor's performance across different respiratory frequencies[39-41]. Throughout each test, data from the soft sensor were collected at a sampling rate of 100 Hz using a data acquisition board and stored on a laptop. Subsequently, these data were processed using MATLAB. In the second proof-of-concept experiment, our sensor was tested in three states: no contact, soft touch, and hard touch. Additionally, three further tasks were carried out: (i) deep tapping, where the subject performed the tapping movement with major force; (ii) slow tapping; (iii) fast tapping; and (iv) tapping as quickly as possible, where the subject was asked to tap as rapidly as possible. All tasks were performed with the index finger of the dominant hand. For the tests, a PLA holder was designed to fix the soft sensor on a horizontal surface.

RESULTS AND DISCUSSION

Characterization of soft pressure sensors

In this study, the first experimental steps involved the design of the pressure sensors, the fabrication and characterization of the materials, the realization of the soft media and the assembly of the entire pressure sensors' structure. The proposed pressure sensors exhibit a soft structure that enables control over the sensor's stiffness, allowing the sensor to offer different measurable pressure ranges by adjusting only its shape and material composition. All soft structures were made with identical external shapes to ensure the consistency of the force application surface. However, the internal shape varied to adjust the structure's stiffness.

Specifically, the FULL shape is the most rigid as it does not have an inner air chamber; the DOM shape has intermediate stiffness due to its structurally efficient shape that evenly distributes stresses and features a smaller inner air chamber than the CIL shape, which has the thinnest walls among the three shapes and the largest inner air chamber, resulting in lower stiffness. The materials of the soft element were also chosen to vary its stiffness. The measured compression Young's values for each material were 81 kPa (Eco50), 71 kPa (Eco30), 47 kPa (Eco30t10), 41 kPa (Eco30t20), and 34 kPa (Eco30t25). Additional information is provided in Supplementary Section 4.

The proposed sensors measure pressure through variations in the distance between the Hall sensor and the magnet. When a force is applied to the surface of the polymeric medium containing the magnet, the medium deforms by an amount that depends on its stiffness (determined by its shape and material). As the magnet moves, the magnetic field interacts with the Hall sensor, causing a change in its output voltage. The distance of the magnet from the Hall sensor determines the measured output voltage, which can be translated into the pressure applied to the soft medium. This is the foundation of the pressure sensor's sensing mechanism.

The component of the magnetic field perpendicular to the Hall sensor generates a measurable Hall voltage expressed with:

$$V_H = \frac{I \cdot B}{n \cdot t \cdot e} \tag{2}$$

where I represents the current flowing through the sensor, B indicates the magnetic flux density, n stands for the density of mobile charges, e is the charge of an electron and t points to the thickness of the sheet of conductive material composing the sensor itself.

To metrologically characterize the sensors, both static and dynamic tests were conducted. From the graph in Figure 2A, it can be observed that the measurable pressure range increases with the stiffness of the soft media, and that the mechanical response is linear throughout the deformation range for the FULL and DOM shapes and for all materials. This is not the case for the CIL shape; however, the mechanical response is linear in the 0%-12.5% deformation range for all shapes and materials. Additionally, the sensor calibration curve [Figure 2B] shows the influence of the shape and material on the maximum pressure value measured under the same deformation. In the initial state, with zero deformation of the soft medium, the sensor output is equal to Vdd/2, indicating its saturation point when the magnet is positioned 2 mm from the Hall sensor. Figure 2C illustrates the voltage measured by the Hall sensor as the soft medium undergoes deformation across various shapes and materials.

This data highlights the sensors' reproducibility, independent of the differences in material composition and shape. The sensitivity values were calculated in the range 0%-37.5% compressive strain as the normalized values of voltage variations ($\frac{\Delta V}{V_0}$, where V_0 is the output voltage at zero pressure) relative to pressure changes ($\widehat{S_\varepsilon}$, as in Equation 3).

$$\widehat{S_\varepsilon} = \frac{\frac{\Delta V}{V_0}}{\Delta P} \tag{3}$$

Overall, the softer materials show higher sensitivity values than the stiffer ones. As shown in Table 1, these values are higher for the softer shapes (max value: CIL shape with Eco30t25, -5.1 × 10^{-2} kPa^{-1}) while they are lower for the stiffer shapes (min value: FULL shape with Eco50, -0.4 × 10^{-2} kPa^{-1}).

These sensitivity values show considerable promise, surpassing those typically achieved by pressure sensors utilizing alternative principles such as piezoresistive technology[42-44]. Furthermore, these sensors exhibit excellent sensitivity across a broad range of measurable pressures, comparing favorably with existing literature findings[31]. Recovery time appears to be independent of both the shape and the material of the soft sensor element. Consequently, it is also independent of the measured pressure range, being approximately 0.4 s for all the sensors [Table 1 and Supplementary Section 5]. This demonstrates the sensors' ability to return to their initial shape after pressure application, making them suitable for many applications requiring measurement of cyclic phenomena. The results are very interesting when compared to sensors based on other operating principles[45-47].

The sensors' output was also evaluated under cyclic loading and unloading cycles at different compression rates (0.1, 0.2, 0.8, and 1 Hz at 25% compression strain) to test their behavior across a wide range of frequencies. The hysteresis error values depend mainly on the compression rate, with no significant difference when varying the shape and material [Table 2]. Specifically, the sensors exhibit higher hysteresis values as the frequency of the cyclic load increases. They range from 2%-6% for compression rates up to 0.2 Hz. For a compression rate of 0.8 Hz, these values increase but remain within the 6%-10% range. Finally, they range from 8%-15% for compression rates of 1 Hz. These values indicate promising sensor behavior when subjected to cyclic loads, making them excellent candidates for numerous applications, such as respiratory monitoring. Additionally, as illustrated in Figure 2D, the V_{out} remains stable after 1,000 load and unload cycles. This demonstrates excellent sensor stability, unlike other pressure sensors, such as piezoresistive pressure sensors that typically show a drift in output[48-50].

Table 1. $\widehat{S}_\varepsilon$ values measured in the sensor full detection range (0%-37.5% strain), and recovery time values calculated per each shape and material

	Eco50	Eco30	Eco30t10	Eco30t20	Eco30t25
FULL shape					
$\widehat{S}_\varepsilon$ [kPa^{-1}]	-0.4×10^{-2}	-0.6×10^{-2}	-0.8×10^{-2}	-0.8×10^{-2}	-1.2×10^{-2}
Recovery time [s]	0.40	0.42	0.41	0.43	0.41
DOM shape					
$\widehat{S}_\varepsilon$ [kPa^{-1}]	-0.8×10^{-2}	-1.2×10^{-2}	-1.5×10^{-2}	-2.3×10^{-2}	-2.5×10^{-2}
Recovery time [s]	0.42	0.41	0.41	0.44	0.42
CIL shape					
$\widehat{S}_\varepsilon$ [kPa^{-1}]	-1.1×10^{-2}	-2.4×10^{-2}	-2.5×10^{-2}	-4.9×10^{-2}	-5.1×10^{-2}
Recovery time [s]	0.46	0.44	0.39	0.44	0.40

Table 2. Hysteresis values obtained per each material and each shape at different compression rates

	Eco50	Eco30	Eco30t10	Eco30t20	Eco30t25
FULL shape					
0.1 Hz	2.74%	2.94%	3.89%	3.03%	3.20%
0.2 Hz	4.89%	5.77%	3.18%	3.06%	5.57%
0.8 Hz	7.46%	6.79%	9.39%	6.90%	8.87%
1 Hz	10.68%	9.02%	8.76%	11.58%	9.64%
DOM shape					
0.1 Hz	2.69%	3.63%	3.63%	3.24%	4.23%
0.2 Hz	4.98%	6.23%	5.12%	4.44%	4.72%
0.8 Hz	8.45%	9.59%	7.50%	9.14%	6.74%
1 Hz	9.89%	12.66%	15.26%	11.69%	12.18%
CIL shape					
0.1 Hz	3.14%	3.59%	4.04%	2.65%	3.14%
0.2 Hz	5.89%	5.93%	4.20%	4.51%	4.34%
0.8 Hz	9.86%	8.98%	7.99%	10.10%	9.70%
1 Hz	11.60%	10.36%	8.66%	13.60%	10.01%

FEM for soft pressure sensors

To analyze the impact of the shape and materials on the sensor's mechanical behavior, a FEM was implemented. The materials used for the soft medium were characterized according to respective standard guidelines. Stress and strain data were calculated [Figure 3A], and then input into the simulation platform, where the Yeoh model determined material coefficients that best fit the experimental data. Subsequently, simulations were conducted considering each sensor's shape and material to study their mechanical behavior [Figure 3B]. To assess the validity of the simulations, a comparison was carried out between the maximum detection limit of pressure values obtained from the FEM and the experimental results on all the samples at 12.5% compression of the soft medium [Figure 3C]. A reasonable discrepancy was found between the simulated and experimental data [Figure 3D], which increases with the sensor's stiffness. However, both simulated and experimental data show an increasing maximum detection limit as the material stiffness increases and the inner chamber size within the soft medium decreases. The simulated pressure values are in the range from 3.29 kPa (Eco30t25) to 8.50 kPa (Eco50) for the CIL shape; range from 4.12 kPa (Eco30t25) to 10.64 kPa (Eco50) for the DOM shape; and range from 5.63 kPa (Eco30t25) to 14.53 kPa (Eco50) for the FULL shape.

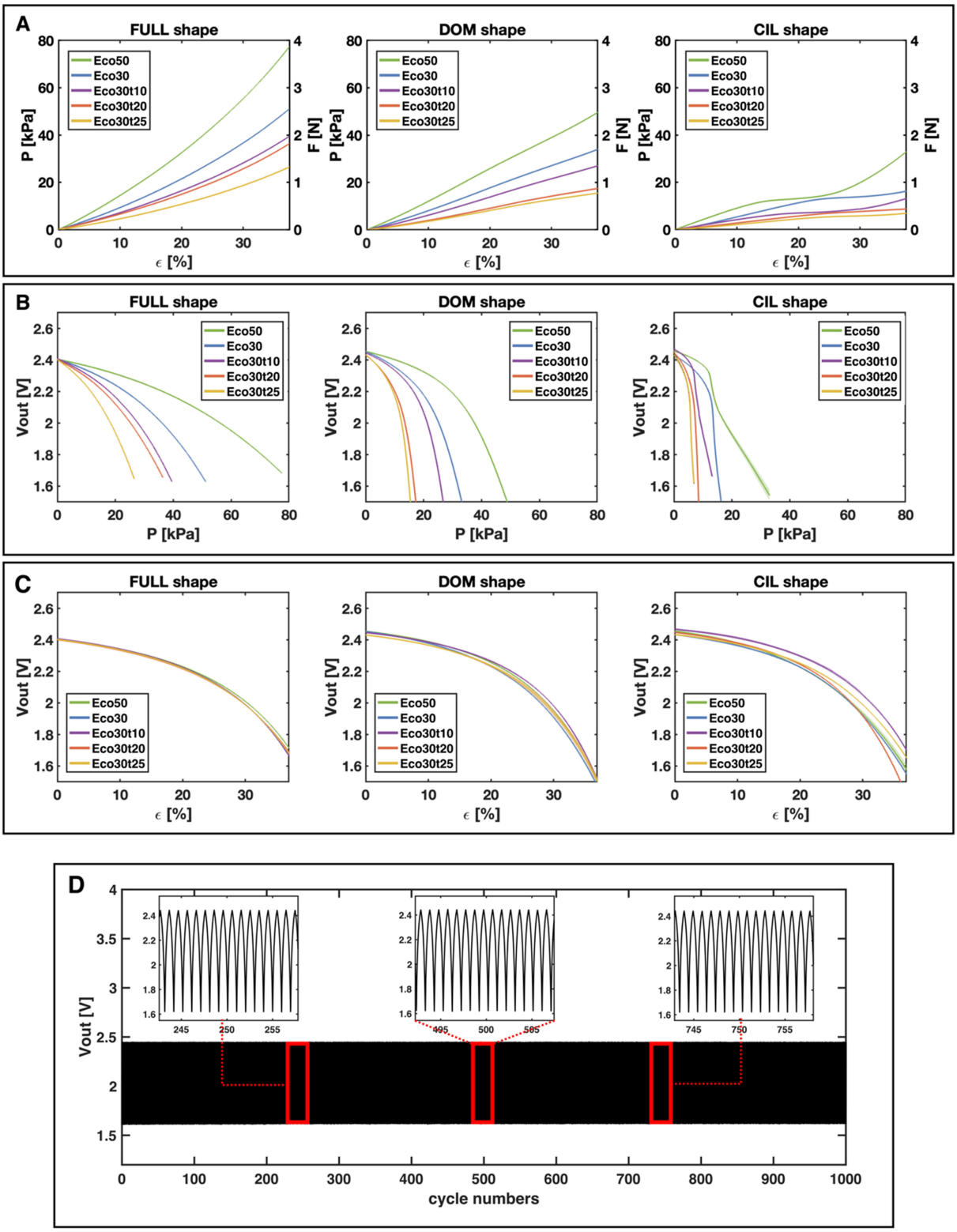

Figure 2. (A) Change in pressure and force applied to the upper surface of the outer cylinder of the soft sensors as a function of deformation for all the shapes and materials of the soft medium. Solid line: average value; filled area: uncertainty; (B) Change in voltage measured by the magnetic pressure sensors as a function of pressure applied to the upper surface for all the shapes and materials of the soft medium. Solid line: average value; filled area: uncertainty; (C) Change in voltage measured by the magnetic pressure sensors as a function of deformation. Solid line: average value; filled area: uncertainty; (D) Voltage variation of the soft pressure sensor with CIL shape and Eco30 after 1,000 loading/unloading cycles at 0.8 Hz.

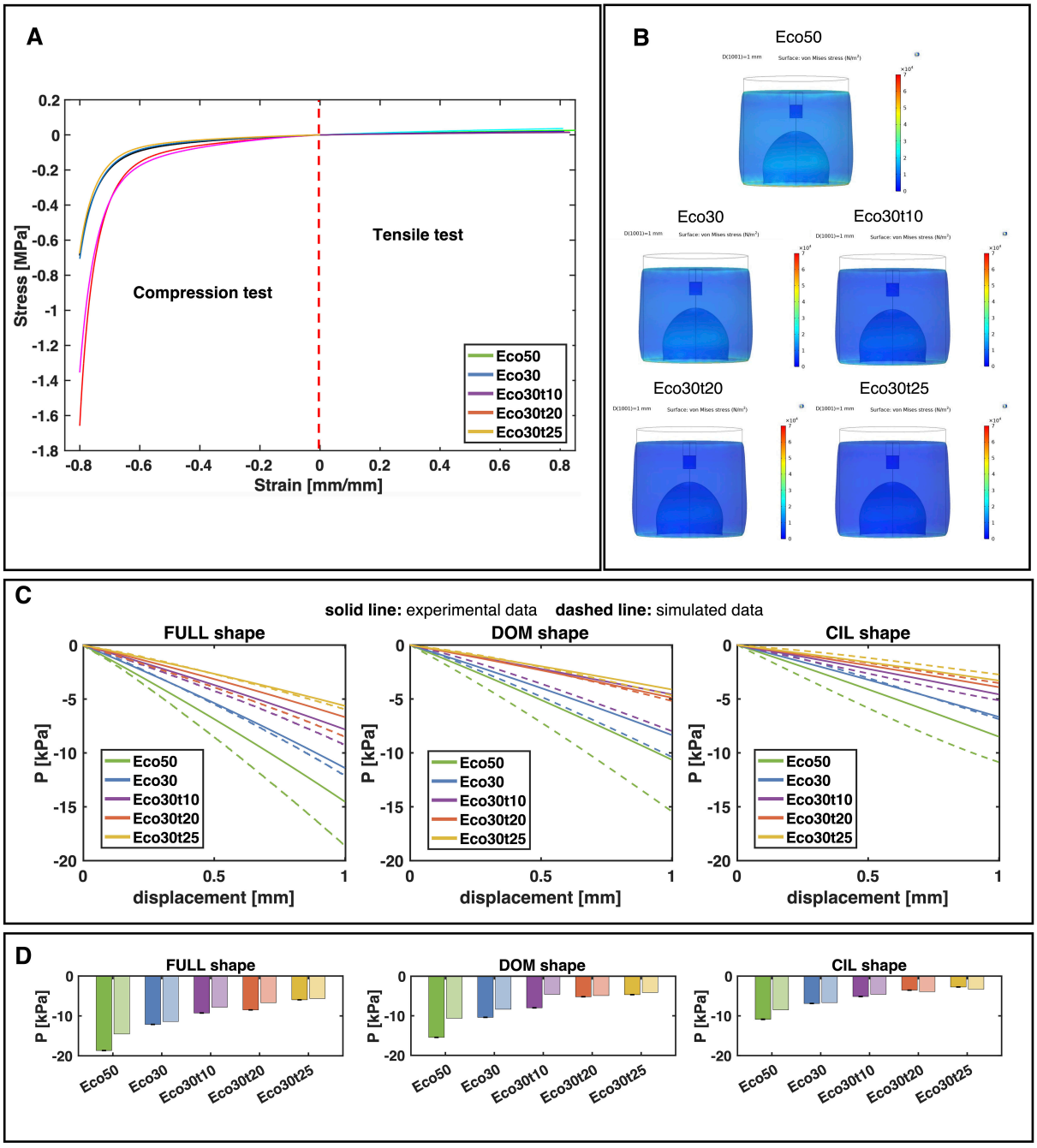

Figure 3. (A) Stress-strain curve obtained for the five materials tested as a result of the combination of tensile and compression tests; (B) Von Mises stress obtained from the FEM simulations for one shape and each material of the soft medium of the magnetic pressure sensors; (C) pressure change measured on the upper surface of the sensors during the experimental tests (solid line) and during the FEM simulations (dashed line) for the different materials and shapes; (D) Maximum pressure detection limit measured during the experimental tests (solid color) with the related uncertainty (black error bar) and during the simulations (color with transparency) for each shape and material of the soft medium. M1: Eco50; M2:Eco30; M3:Eco30t10; M4:Eco30t20; M5:Eco30t25. FEM: Finite Element Method.

Breathing and finger-tapping detection through soft pressure sensors

To demonstrate the sensors' effectiveness and adaptability to different applications, they were used for physiological parameter monitoring and tactile sensing. Two proof-of-concept experiments were carried

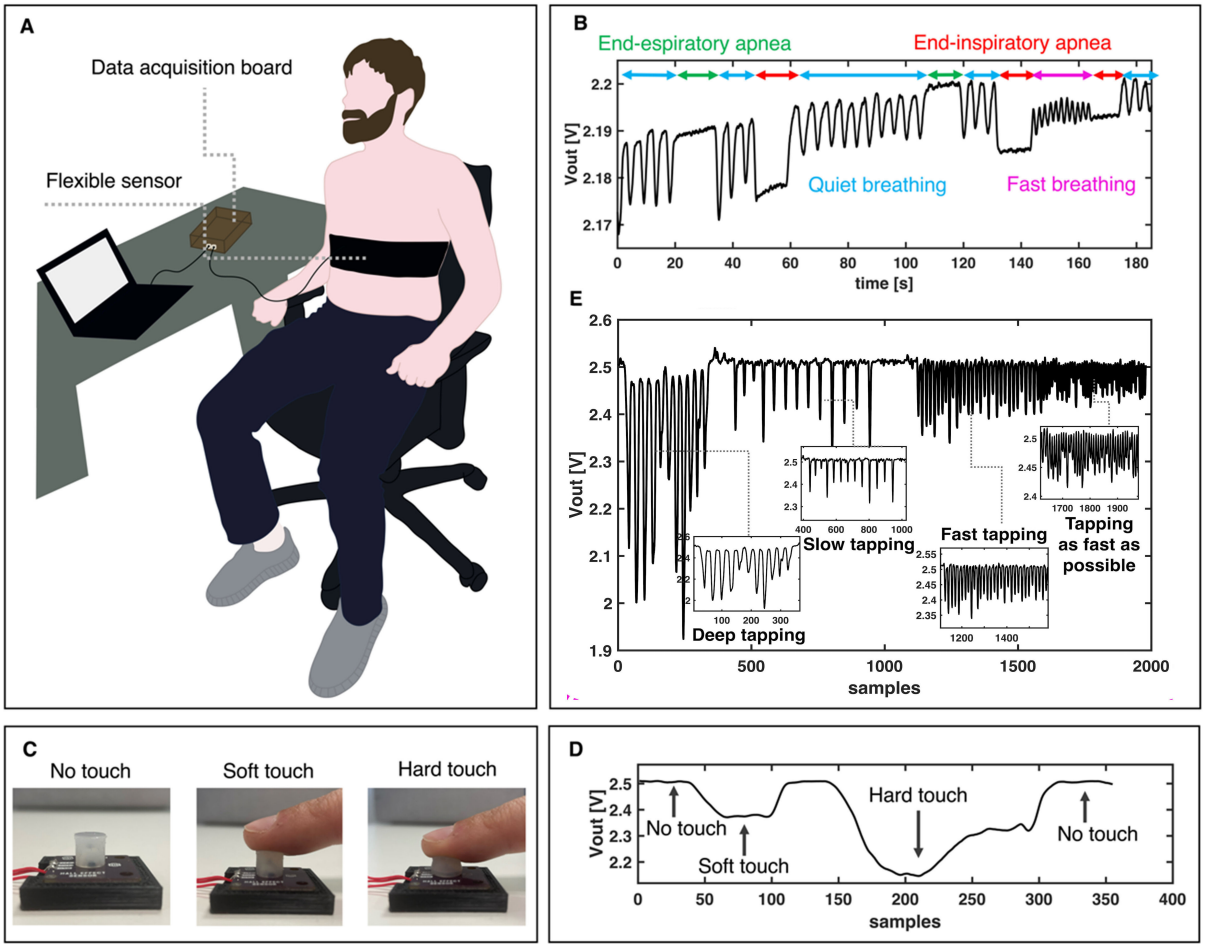

Figure 4. (A) Representation of the experimental setup including the CIL shape Eco30 sensor placed in a chest strap worn by the subject; (B) Respiratory signal collected during the breathing test showing the different phases of the protocol including slow and fast breathing and apnea phases; (C) Experimental setup used during the tapping test; (D) Signal collected during the tapping test, in the absence of touching the sensor with the finger, when a soft touch is applied and when a hard touch is applied; (E) Signal collected during the tapping test which includes deep tapping, slow tapping fast tapping and tapping as fast as possible.

out. The first test involved using the soft sensors for respiratory monitoring, providing critical information on a patient's breathing patterns and overall respiratory health. Breathing frequency can also provide useful information about a subject's psychophysical state. Accurate measurement of various respiratory rates and detection of apnea is essential for diagnosing and managing conditions such as obstructive sleep apnea[51,52], helping to prevent complications, ensuring timely interventions[53], and improving patient outcomes[54] and athletes training[55,56]. The sensor was integrated into a wearable chest strap for breathing monitoring [Figure 4A]. We measured the pressure exerted by the sternum while breathing. The sensor provided a pattern where each respiratory cycle (inhalation-exhalation) had an increasing phase, a maximum peak, and a decreasing phase. Pilot experiments were carried out on a healthy volunteer (male, 35 years old) to investigate the sensors' ability to estimate breathing from chest wall movements. The rib cage movements during breathing apply force to the soft medium of the sensors, causing magnet displacement and a change in the Hall sensor output. For this purpose, the CIL shape Eco30 sensor was embedded into a wearable band using double-sided Velcro. This sensor was selected for its balance between sensitivity and hysteresis, relevant for respiratory monitoring. The soft part of the sensor was positioned toward the subject's chest, centered on the sternum at the height of the seventh rib.

The volunteer followed an experimental protocol that included different breathing rates and depths. All protocol steps were performed to investigate the functionality of the pressure sensors at different respiratory frequencies within the physiological range. As shown in Figure 4B, the data collected with the proposed sensor allow the identification of slow breathing, and fast breathing phases. The apnea phases are also identifiable in the signals, shown by an almost constant signal throughout the apnea duration. End-inspiratory and end-expiratory apnea can be distinguished by their different mean values. This feature could be crucial for devices studying apnea, not found in many respiratory monitoring devices[57]. The minimum thickness achieved in this real-life application is 6.1 mm.

The second proof-of-concept experiment measured tapping, useful in numerous applications including the evaluation of muscle control or the assessment of patient recovery after a stroke[58]. Movements are typically monitored in amplitude, rhythm, and speed to assess disorders such as muscle tremor and rigidity[59].

We measured the pressure exerted on the sensor by the impact of the finger at different speeds and intensities. Specifically, our sensor was tested under three conditions: no contact, soft touch, and hard touch [Figure 4C]. Figure 4D shows the output voltage in soft touch, hard touch and no touch phases, easily distinguishable. Then, the sensor was evaluated during four additional tasks: deep tapping with maximum force, slow tapping, fast tapping, and tapping as fast as possible. Figure 4E shows the sensor output at different tapping frequencies. Regardless of the tapping frequency, the sensor always returns to its initial value in the absence of pressure, showing good repeatability. The minimum thickness achieved in this real-life application is 5.6 mm.

The results from these tests demonstrate the sensors' ability to follow both slow (e.g., touch and breath during apnea and quiet breathing) and rapid phenomena (e.g., tapping or breathing during tachypnoea).

CONCLUSIONS

This study introduces a novel approach to designing and fabricating soft pressure sensors with tunable stiffness, offering adaptability across various applications. We developed and characterized sensors capable of detecting medium and low-pressure ranges. Our sensor employs a magnetic sensing mechanism, where deformation of a soft polymeric medium induces changes in magnetic field intensity, allowing for measurement of applied pressure.

Our findings reveal significant variations in sensor performance based on shape and material composition. Sensitivity values range from 0.4×10^{-2} to 5.1×10^{-2} kPa^{-1} across different configurations. Moreover, the sensors exhibit a wide range of maximum detectable pressure values, up to 77.4 kPa, depending on the stiffness of the material and the sensor's shape. Experimental tests demonstrated the sensor's robust performance under both static and dynamic loading conditions. The sensors also show a promising recovery time of 0.4 s, making it suitable for real-time pressure monitoring. Table 3 compares our sensor with similar sensor technologies.

We tested the sensors in two different application fields to demonstrate their versatility. One sensor was tested for respiratory monitoring during normal breathing and high-frequency breathing (tachypnoea). It demonstrated the sensor's ability to follow rapid and minimal changes well. An important feature of our sensors is their monoaxial design, which primarily detects magnet movements perpendicular to the Hall sensor (z-axis). This design is expected to reduce susceptibility to motion artifacts during activities such as walking, where magnet movements predominantly occur in the xy-plane.

Table 3. Comparison of pressure sensors

Sensing area	Working principle	Sensitivity	Recovery time	Measuring range	Ref.
15 × 15 mm^2	Capacitive	0.161 kPa^{-1}	N.D.	0-10 kPa	[4]
6 × 6 mm^2	Capacitive	0.000022 kPa^{-1}	N.D.	240-1,000 kPa	[32]
N.D.	Capacitive	0.01 kPa^{-1}	800 ms	18-70 kPa	[22]
10 × 10 mm^2	Piezoresistive	0.096 kPa^{-1}	N.D.	0-175 kPa	[60]
28 × 28 mm^2	Piezoresistive	0.011 kPa^{-1}	N.D.	0-120 kPa	[24]
56 mm^2	Magnetic	16 mV/N	N.D.	0-0.05 kPa	[33]
50 mm^2	Magnetic	-0.051 kPa^{-1}	400 ms	0-7 kPa	Our work: CIL, Eco30t25
50 mm^2	Magnetic	-0.004 kPa^{-1}	400 ms	0-80 kPa	Our work: FULL Eco50

N.D.: Not declared.

Future research will involve comprehensive testing to assess the sensor's performance and susceptibility to motion artifacts in real-life applications. This includes analyzing its behavior during various activities and comparing it with other sensor types to establish robustness and reliability. Another sensor was tested during tapping at different frequencies and intensities, demonstrating strong adaptability to various operating conditions. Overall, the sensors presented in this work demonstrate significant potential for miniaturization and customization to specific applications. The dimensions of the current design can be reduced by optimizing the geometry, materials, and magnetization of the sensor components. This miniaturization will enhance user comfort and expand its applicability in wearable and robotic devices.

DECLARATIONS

Authors' contributions

Conceived the concept of the magnetic pressure sensors tunable by hyperplastic materials mediums and supervised the project: Massaroni C

Designed the pressure sensors and conducted all the experiments: Romano C, Lo Presti D, Massaroni C

Provided support throughout the experiment process and revised the manuscript: Silvestri S, Schena E

Contributed to discussions regarding the performance and analysis of the architected pressure sensors: Romano C, Lo Presti D, Massaroni C

Participated in writing: Romano C, Massaroni C

Availability of data and materials

The datasets, including experimental data and simulation models presented in this study, and the code used and presented in this study are available upon request from the corresponding author.

Financial support and sponsorship

The authors acknowledge the financial support from European Union-Next Generation EU-NRRP M4.C2-Investment 1.5 Establishing and Strengthening of Innovation Ecosystems for Sustainability (Rome Technopole) under Project ECS00000024.

Conflicts of interest

Massaroni C is the guest editor of the special issue, while the other authors have declared that they have no conflicts of interest.

Ethical approval and consent to participate

This study was conducted in compliance with the Declaration of Helsinki's guidelines and received approval from the Università Campus Bio-Medico di Roma's Institutional Ethics Committee (09/19 OSS ComEt

UCBM). All participants were informed about the experimental procedure and research purposes, and have signed the relevant consent forms prior to participation.

Consent for publication

Participants have been informed that their detailed information and images will be used for the purpose of this study. They have also signed written consent forms allowing those details to be published.

Copyright

REFERENCES

1. Xu C, Chen J, Zhu Z, et al. Flexible pressure sensors in human-machine interface applications. *Small* 2024;20:e2306655. DOI PubMed
2. Shi L, Li Z, Chen M, Zhu T, Wu L. Ultrasensitive and ultraprecise pressure sensors for soft systems. *Adv Mater* 2023;35:e2210091. DOI PubMed
3. Li J, Jia H, Zhou J, et al. Thin, soft, wearable system for continuous wireless monitoring of artery blood pressure. *Nat Commun* 2023;14:5009. DOI PubMed PMC
4. Park SW, Das PS, Chhetry A, Park JY. A flexible capacitive pressure sensor for wearable respiration monitoring system. *IEEE Sensors J* 2017;17:6558-64. DOI
5. Zulkifli NA, Jeong W, Kim M, et al. 3D-printed magnetic-based air pressure sensor for continuous respiration monitoring and breathing rehabilitation. *Soft Sci* 2024;4:20. DOI
6. Park Y, Luan H, Kwon K, et al. Soft, full Wheatstone bridge 3D pressure sensors for cardiovascular monitoring. *npj Flex Electron* 2024;8:294. DOI
7. Dahiya RS, Metta G, Valle M, Sandini G. Tactile sensing - from humans to humanoids. *IEEE Trans Robot* 2010;26:1-20. DOI
8. Jan AA, Kim S, Kim S. A skin-wearable and self-powered laminated pressure sensor based on triboelectric nanogenerator for monitoring human motion. *Soft Sci* 2024;4:10. DOI
9. De Tommasi F, Lo Presti D, Virgili F, Massaroni C, Schena E, Carassiti M. Soft system based on fiber bragg grating sensor for loss of resistance detection during epidural procedures: in silico and in vivo assessment. *Sensors* 2021;21:5329. DOI PubMed PMC
10. Bandari N, Dargahi J, Packirisamy M. Tactile sensors for minimally invasive surgery: a review of the state-of-the-art, applications, and perspectives. *IEEE Access* 2020;8:7682-708. DOI
11. Tian S, Wang Y, Deng H, Wang Y, Zhang X. Flexible pressure and temperature sensors towards e-skin: material, mechanism, structure and fabrication. *Soft Sci* 2023;3:30. DOI
12. Sun G, Wang P, Jiang Y, Sun H, Meng C, Guo S. Recent advances in flexible and soft gel-based pressure sensors. *Soft Sci* 2022;2:17. DOI
13. Tian H, Shu Y, Wang XF, et al. A graphene-based resistive pressure sensor with record-high sensitivity in a wide pressure range. *Sci Rep* 2015;5:8603. DOI PubMed PMC
14. Cao Y, Li J, Dong Z, et al. Flexible tactile sensor with an embedded-hair-in-elastomer structure for normal and shear stress sensing. *Soft Sci* 2023;3:32. DOI
15. Zhang Y, Liu C, Jia B, et al. Kirigami-inspired, three-dimensional piezoelectric pressure sensors assembled by compressive buckling. *npj Flex Electron* 2024;8:310. DOI
16. Huang Y, Liu B, Zhang W, et al. Highly sensitive active-powering pressure sensor enabled by integration of double-rough surface hydrogel and flexible batteries. *npj Flex Electron* 2022;6:226. DOI
17. Pruvost M, Smit WJ, Monteux C, Poulin P, Colin A. Polymeric foams for flexible and highly sensitive low-pressure capacitive sensors. *npj Flex Electron* 2019;3:52. DOI
18. Liu J, Tian G, Yang W, Deng W. Recent progress in flexible piezoelectric devices toward human-machine interactions. *Soft Sci* 2022;2:22. DOI
19. Kim KH, Kim JH, Ko YJ, Lee HE. Body-attachable multifunctional electronic skins for bio-signal monitoring and therapeutic applications. *Soft Sci* 2024;4:24. DOI
20. Lee JH, Yoon HJ, Kim TY, et al. Micropatterned P(VDF-TrFE) film-based piezoelectric nanogenerators for highly sensitive self-powered pressure sensors. *Adv Funct Mater* 2015;25:3203-9. DOI
21. Park J, Lee Y, Hong J, et al. Giant tunneling piezoresistance of composite elastomers with interlocked microdome arrays for ultrasensitive and multimodal electronic skins. *ACS Nano* 2014;8:4689-97. DOI
22. Moeinnia H, Agron DJ, Ganzert C, Schubert L, Kim WS. Wireless pressure monitoring system utilizing a 3D-printed Origami pressure sensor array. *npj Flex Electron* 2024;8:309. DOI
23. Liu H, Huang W, Gao J, et al. Piezoresistive behavior of porous carbon nanotube-thermoplastic polyurethane conductive nanocomposites with ultrahigh compressibility. *Appl Phys Lett* 2016;108:011904. DOI

24. Park YJ, Sharma BK, Shinde SM, et al. All MoS_2-based large area, skin-attachable active-matrix tactile sensor. *ACS Nano* 2019;13:3023-30. DOI PubMed
25. Massaroni C, Vitali L, Lo Presti D, Silvestri S, Schena E. Fully additively 3D manufactured conductive deformable sensors for pressure sensing. *Adv Intell Syst* 2024;6:2300901. DOI
26. Hu J, Dun G, Geng X, Chen J, Wu X, Ren TL. Recent progress in flexible micro-pressure sensors for wearable health monitoring. *Nanoscale Adv* 2023;5:3131-45. DOI PubMed PMC
27. Chun J, Lee KY, Kang CY, Kim MW, Kim SW, Baik JM. Embossed hollow hemisphere-based piezoelectric nanogenerator and highly responsive pressure sensor. *Adv Funct Mater* 2014;24:2038-43. DOI
28. Chi C, Sun X, Xue N, Li T, Liu C. Recent progress in technologies for tactile sensors. *Sensors* 2018;18:948. DOI PubMed PMC
29. Metzger C, Fleisch E, Meyer J, et al. Flexible-foam-based capacitive sensor arrays for object detection at low cost. *Appl Phys Lett* 2008;92:013506. DOI
30. He F, Huang Q, Qin M. A silicon directly bonded capacitive absolute pressure sensor. *Sens Actuators A Phys* 2007;135:507-14. DOI
31. Wang X, Yu J, Cui Y, Li W. Research progress of flexible wearable pressure sensors. *Sens Actuators A Phys* 2021;330:112838. DOI
32. Lei KF, Lee K, Lee M. A flexible PDMS capacitive tactile sensor with adjustable measurement range for plantar pressure measurement. *Microsyst Technol* 2014;20:1351-8. DOI
33. Rehan M, Saleem MM, Tiwana MI, Shakoor RI, Cheung R. A soft multi-axis high force range magnetic tactile sensor for force feedback in robotic surgical systems. *Sensors* 2022;22:3500. DOI PubMed PMC
34. Jiao J, Guo Y, Tong Q, et al. Stiffness-tunable and shape-locking soft actuators based on 3D-printed hybrid multi-materials. *Soft Sci* 2022;2:20. DOI
35. Lin X, Han M. Recent progress in soft electronics and robotics based on magnetic nanomaterials. *Soft Sci* 2023;3:14. DOI
36. Nguyen TV, Mizuki Y, Tsukagoshi T, Takahata T, Ichiki M, Shimoyama I. MEMS-based pulse wave sensor utilizing a piezoresistive cantilever. *Sensors* 2020;20:1052. DOI PubMed PMC
37. Kubba AE, Hasson A, Kubba AI, Hall G. A micro-capacitive pressure sensor design and modelling. *J Sens Sens Syst* 2016;5:95-112. DOI
38. Parameswaran C, Gupta D. Large area flexible pressure/strain sensors and arrays using nanomaterials and printing techniques. *Nano Converg* 2019;6:28. DOI PubMed PMC
39. Romano C, Nicolò A, Innocenti L, et al. Respiratory rate estimation during walking and running using breathing sounds recorded with a microphone. *Biosensors* 2023;13:637. DOI
40. Romano C, Formica D, Schena E, Massaroni C. Investigation of body locations for cardiac and respiratory monitoring with skin-interfaced inertial measurement unit sensors. *IEEE Sensors J* 2023;23:7806-15. DOI
41. Romano C, Schena E, Silvestri S, Massaroni C. Non-contact respiratory monitoring using an RGB camera for real-world applications. *Sensors* 2021;21:5126. DOI PubMed PMC
42. Rinaldi A, Tamburrano A, Fortunato M, Sarto MS. A flexible and highly sensitive pressure sensor based on a PDMS foam coated with graphene nanoplatelets. *Sensors* 2016;16:2148. DOI PubMed PMC
43. Wei Y, Chen S, Lin Y, Yuan X, Liu L. Silver nanowires coated on cotton for flexible pressure sensors. *J Mater Chem C* 2016;4:935-43. DOI
44. Massaroni C, Vitali L, Presti Lo D, Silvestri S, Schena E. Design, development and characterization of a novel fully additively manufactured deformable conductive force sensor. In: 2023 International Workshop on Biomedical Applications, Technologies and Sensors (BATS); 2023 Sep 28-29; Catanzaro, Italy. IEEE; 2023. pp. 22-7. DOI
45. Yuan J, Li Q, Ding L, et al. Carbon black/multi-walled carbon nanotube-based, highly sensitive, flexible pressure sensor. *ACS Omega* 2022;7:44428-37. DOI PubMed PMC
46. Zhang F, Yang K, Pei Z, et al. A highly accurate flexible sensor system for human blood pressure and heart rate monitoring based on graphene/sponge. *RSC Adv* 2022;12:2391-8. DOI PubMed PMC
47. Fu J, Taher SE, Abu Al-rub RK, Zhang T, Chan V, Liao K. Engineering 3D-architected gyroid MXene scaffolds for ultrasensitive micromechanical sensing. *Adv Eng Mater* 2022;24:2101388. DOI
48. Qi Z, Zhang T, Zhang X, Xu Q, Cao K, Chen R. MXene-based flexible pressure sensor with piezoresistive properties significantly enhanced by atomic layer infiltration. *Nano Mater Sci* 2023;5:439-46. DOI
49. Zheng S, Wu X, Huang Y, et al. Highly sensitive and multifunctional piezoresistive sensor based on polyaniline foam for wearable Human-Activity monitoring. *Compos Part A Appl Sci Manuf* 2019;121:510-6. DOI
50. Kang F, Zhang W, Liu M, Liu F, Jia Z, Jia D. Highly flexible and sensitive Ti_3C_2 MXene@polyurethane composites for piezoresistive pressure sensor. *J Mater Sci* 2022;57:12894-902. DOI
51. Nicolò A, Massaroni C, Schena E, Sacchetti M. The importance of respiratory rate monitoring: from healthcare to sport and exercise. *Sensors* 2020;20:6396. DOI PubMed PMC
52. Masaoka Y, Homma I. Anxiety and respiratory patterns: their relationship during mental stress and physical load. *Int J Psychophysiol* 1997;27:153-9. DOI PubMed
53. Tarassenko L, Hann A, Young D. Integrated monitoring and analysis for early warning of patient deterioration. *Br J Anaesth* 2006;97:64-8. DOI PubMed
54. Lamberti JP. Respiratory monitoring in general care units. *Respir Care* 2020;65:870-81. DOI PubMed
55. Romano C, Innocenti L, Schena E, Sacchetti M, Nicolò A, Massaroni C. A signal quality index for improving the estimation of breath-

by-breath respiratory rate during sport and exercise. *IEEE Sensors J* 2023;23:31250-8. DOI

56. Innocenti L, Romano C, Greco G, et al. Breathing monitoring in soccer: part I - validity of commercial wearable sensors. *Sensors* 2024;24:4571. DOI PubMed PMC
57. Massaroni C, Nicolò A, Lo Presti D, Sacchetti M, Silvestri S, Schena E. Contact-based methods for measuring respiratory rate. *Sensors* 2019;19:908. DOI PubMed PMC
58. de Groot-Driessen D, van de Sande P, van Heugten C. Speed of finger tapping as a predictor of functional outcome after unilateral stroke. *Arch Phys Med Rehabil* 2006;87:40-4. DOI PubMed
59. Lee M, Jeong JH, Kim YH, Lee SW. Decoding finger tapping with the affected hand in chronic stroke patients during motor imagery and execution. *IEEE Trans Neural Syst Rehabil Eng* 2021;29:1099-109. DOI
60. Tang Z, Jia S, Zhou C, Li B. 3D printing of highly sensitive and large-measurement-range flexible pressure sensors with a positive piezoresistive effect. *ACS Appl Mater Interfaces* 2020;12:28669-80. DOI